JOURNAL OF APPLIED PHYSICS 109, 074310 (2011)

Tuning of the surface plasmon resonance in TiO_2/Au thin films grown by magnetron sputtering: The effect of thermal annealing

M. Torrell,[1,a)] R. Kabir,[1] L. Cunha,[1] M. I. Vasilevskiy,[1] F. Vaz,[1] A. Cavaleiro,[2] E. Alves,[3] and N. P. Barradas[3]
[1]*Centro de Física, Universidade do Minho, 4710-057 Braga, Portugal*
[2]*Departamento de Engenharia Mecânica, SEC-CEMUC, Universidade de Coimbra, Polo II, 3030-788 Coimbra, Portugal*
[3]*Instituto Tecnológico e Nuclear, Departamento de Física, 2686-953 Sacavém, Portugal*

Nanocomposites consisting of a dielectric matrix, such as TiO_2, with embedded noble metal nanoparticles (NPs) possess specific optical properties due to the surface plasmon resonance (SPR) effect, interesting for several applications. The aim of this work is to demonstrate that these properties are sensitive to the nanostructure of magnetron-sputtered TiO_2/Au thin films, which can be tuned by annealing. We study the role of the shape and size distribution of the NPs, as well as the influence of the crystallinity and phase composition of the host matrix on the optical response of the films. All these characteristics can be modified by vacuum annealing treatments of the deposited films. A theoretical interpretation and modeling of the experimental results obtained is presented. The model involves a modified Maxwell-Garnett approach for the effective dielectric function of the composite (describing the SPR effect) and the transfer matrix formalism for multilayer optics. Input data are based on the experimental information obtained from the detailed structural characterization of the films. It is shown that the annealing treatments can be used for controlling the optical properties of the composite films, making them attractive for decorative coatings. © *2011 American Institute of Physics*. [doi:10.1063/1.3565066]

I. INTRODUCTION

The interest in composite materials containing metal nanoparticles (NPs) embedded in dielectric matrices is related to their potential for a wide range of advanced technological applications. To begin with, noble metal NPs have provided different colors in Roman glasses and windows of medieval cathedrals for centuries. Modern applications include color filters,[1] bio- and optical sensors,[2–4] absorption elements of solar cells,[3] enhancement of electrical/thermal conductivity of coatings, photocatalytic antibacterial[5] and pollutant-degradation materials,[6–8] and gas sensors.[9,10] NP composites are also considered for nonlinear optical properties[3,11,12] and surface enhanced Raman scattering (SERS) effect.[13] Most of these applications, in particular, those belonging to the decorative field, rely on the so called surface plasmon resonance (SPR) absorption, which is governed by the type of the metal, the morphology of NPs, and the dielectric properties of the medium where the NPs are dispersed.[14–17]

SPR in small metallic particles is generated by collective oscillations of the free electrons, induced by external electromagnetic radiation. Its spectral characteristics depend on both the NPs and host matrix properties. Let us recall the essential SPR features in a single metallic particle embedded in a dielectric matrix. Considering a perfectly spherical particle and the dipole approximation of the Mie theory[18] (valid when the radiation wavelength, λ, is much larger than the particle radius, R), the SPR condition is

$$\varepsilon_s + 2\varepsilon_h = 0, \tag{1}$$

where ε_h is the dielectric constant of the host (matrix) and ε_s denotes the dielectric function of the metal. In the simple Drude model,

$$\varepsilon_s(\omega) = \varepsilon_\infty \left[1 - \frac{\omega_p^2}{\omega\left(\omega + i\Gamma_p\right)}\right], \tag{2}$$

where ε_∞ is a positive constant, Γ_p is a plasmon damping parameter (proportional to the electron scattering rate) and $\omega_p = \sqrt{4\pi n e^2/(\varepsilon_\infty m^*)}$ is the plasma frequency (n is free electron concentration and m^* is the effective mass). Then, assuming $\Gamma_p << \omega_p$, it follows from Eqs. (1) and (2) that the SPR frequency for a spherical NP is given by

$$\omega_{SPR} = \frac{\omega_p}{\sqrt{1 + 2\varepsilon_h/\varepsilon_\infty}}. \tag{3}$$

It follows from Eq. (3) that the SPR spectral position is independent of the NPs size, but does depend on the dielectric constant of the host. In order to achieve SPR in the visible range, one is practically limited to the noble metals and still has to use host materials with sufficiently high dielectric constant. The width of the resonance is proportional to Γ_p which should increase for smaller particles because an additional scattering mechanism (called surface scattering) becomes more important as R decreases. The intensity of the resonance is proportional to the particle volume.

a)Electronic mail: mtorrellfaro@gmail.com.

SPR properties are affected by the shape and orientation of the particles in the matrix if they are not spherical.[19] For example, axial-symmetric nanorods are expected to produce two SPRs, with the characteristic frequencies given by

$$\omega_{SPR}^{l} = \frac{\omega_p}{\sqrt{1+\left(\eta_{||}^{-1}-1\right)\varepsilon_h/\varepsilon_\infty}};$$
$$\omega_{SPR}^{tr} = \frac{\omega_p}{\sqrt{1+(\eta_{\perp}^{-1}-1)\varepsilon_h/\varepsilon_\infty}}; \quad (4)$$

where $\eta_{||}$ and $\eta_{\perp}$ are so called depolarization coefficients,[20] which are geometrical non-negative factors that obey the relation $\eta_{||} + 2\eta_{\perp} = 1$. If nanorods are embedded in a matrix in a random-orientation way, then one should expect to observe both SPR peaks.

Inter-particle spacing (i.e., the particle concentration) can also have an effect on the SPR intensity, peak position and width. It is related to the electromagnetic interaction (mostly dipole-dipole) between the particles. These effects become considerable when the volume fraction of the particles is above ≈10%. Both theory[18] and experiment[21] indicate that increased volume fraction of gold NPs raises the SPR intensity and leads to a redshift of the position of the resonance.

Thus, for a given metal, there are several means for tuning the SPR spectral properties, namely, (1) dielectric constant of the matrix, (2) NP shape, (3) NP concentration, and, to some extent, (4) NP size. In this work, we study these possibilities both experimentally, using thermal annealing of magnetron-sputtered TiO_2/Au thin films, and theoretically. The paper is organized as follows. The next section presents experimental details concerning the preparation of the samples and the techniques used for their structural characterization. Section III is devoted to the experimental results. In Sec. IV we present the theoretical approach and modeled optical spectra. The last section contains discussion and conclusions.

II. EXPERIMENTAL DETAILS

TiO_2 films were deposited on glass/quartz substrates and *in situ* Au doped by reactive magnetron co-sputtering. One step deposition has been used to produce the host dielectric matrix (TiO_2) and the gold NPs, in a single process. For this, the films were grown using two vertically opposed rectangular magnetrons (unbalanced of type 2) placed in a closed field configuration in the deposition chamber. Only one electrode was powered, composed of a titanium target (99.6% purity), with 8 Au pellets (with a 40 mm^2 surface area and ~2 mm thickness) symmetrically incrusted in the erosion zone. A constant dc current density of 100 A m^{-2} was applied. Argon and oxygen were used to produce the gas mixture, 60 sccm (3×10^{-1} Pa) and 10 sccm (8×10^{-2} Pa), respectively. The deposition temperature was kept approximately constant at a value of about 150 °C. The temperature of the coated substrates was monitored with a thermocouple placed close to the surface of the substrate holder. A delay time of 5 min was used before positioning the surface of the samples in front of the target. This delay time was used to avoid target poisoning resulting from previous depositions and also to assure a practically constant deposition temperature of the substrates during film growth. These conditions produce an approximately constant working pressure of 3.8×10^{-1} Pa during the deposition process. The substrate holder was placed in rotation at 6 rpm and in grounded conditions.

The Au-doped films were annealed, in vacuum, after the deposition. Annealing treatments were carried out in a secondary vacuum furnace, after its evacuation to about 10^{-4} Pa. The annealing temperature range was fixed from 200 to 800 °C, and the isothermal period was fixed at 60 min, after the required heating ramp of 5 °C/min. The samples cooled down freely in vacuum before their removal to room conditions. The films annealed at temperatures above 400 °C were deposited on quartz substrates since it is more stable than glass at elevated temperatures. The purpose of these annealing treatments was to promote the diffusion mechanisms in order to affect NP size, shape, and spatial distribution.

The atomic composition of the as-deposited samples was measured by Rutherford Backscattering Spectroscopy (RBS) using (1.4, 1.75) MeV and 2 MeV for the proton and ^4He beams, respectively. The scattering angles were 140° (standard detector, IBM geometry) and 180° (annular detector), tilt angles 0° and 30°. Composition profiles for the as-deposited samples were generated using the software NDF.[22] For the ^{16}O data, the cross-sections given by Ramos *et al.*[23] were used. The analyzed area was about 0.5 × 0.5 mm^2. In addition, for some samples, Particle Induced X-ray Emission (PIXE) measurements were performed to check for impurities.[22]

The crystalline structure of the TiO_2 matrix and Au nanoclusters as well as the NP size were investigated by X-ray diffraction (XRD) using a Philips PW 1710 diffractometer (Cu-K_α radiation) operating in a Bragg-Brentano configuration. The XRD patterns were deconvoluted assuming the Voigt functions in order to yield the peak position, integrated intensity and integrated width (IntW). The average NP size was determined by three different methods (Integral Breath, Fourier Analysis, and Scherrer formula) using the Au-FCC (111) peak in the XRD patterns.

The thickness and morphology of the films were studied by NanoSEM FEI Nova 200 scanning microscopy and transmission electron microscopy (TEM) using a Hitachi 800H apparatus. TEM microscopy was used also to characterize the shape, size, and distribution of Au NPs with respect to the annealing temperature.

III. EXPERIMENTAL RESULTS

Optical transmission spectroscopy measurements have been carried out in order to study the SPR effect in the TiO_2/Au samples prepared. The spectra presented in Fig. 1 show that the overall transmission decreases with the increase of the annealing temperature, corresponding to an enhanced absorption due to the formation of Au NPs. The morphological changes can be observed by comparing the planar view TEM images of the as deposited samples (Fig. 2(a)) and those annealed at 500 °C (Fig. 2(b)) and 700 °C (Fig. 2(c)), revealing the coalescence of small atomic Au clusters into nanoparticles. In fact, in the as-deposited sample clusters

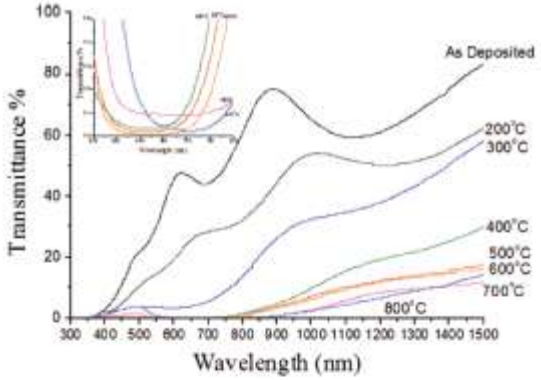

FIG. 1. (Color online) Transmission spectra of the TiO_2/Aufilms on SiO_2 substrates annealed at different temperatures. The inset shows a zoom into the SPR absorption region.

consisting of only few Au atoms are spread all over the entire coating volume. Their coalescence, promoted by the annealing, tends to form well defined Au NPs homogenously dispersed in the dielectric matrix. Beyond this morphological change, onset of a composition gradient could be expected due to enhanced Au diffusion into the substrate. However, it is not seen until the 800 °C annealing temperature as revealed by the RBS analysis (Fig. 3). For temperatures up to 700 °C, the composition profile analysis indicates that the samples are practically homogeneous across the film thickness. These results can have an influence on the optical properties of the films.

Taking into account the observed compositional and morphological changes and the specific optical behavior (including the surface color tones) of the as-deposited and annealed samples, three different groups of TiO_2/Au films can be distinguished as depicted in Fig. 4. The SPR position and grain size for the zone I samples are not presented due to the absence of any noticeable SPR absorption band in the optical spectra of these films and their predominantly amorphous structure (no XRD peak fitting was possible). These two samples are practically transparent and present clear interference fringes. This correlates with the TEM data of Fig. 2(a) where only a few Au atomic clusters are observed, and also with the XRD data presented in Fig. 5 where no diffraction pattern is seen for these samples.

The interference fringes start to disappear in the spectra of samples annealed at temperatures higher than 200 °C. These samples belong to the second group (zone II in Fig. 4), where the Au cluster growth takes place. Although the transmittance spectrum of the 300 °C sample still shows some interference structure, a transmittance minimum close to the 610–620 nm can be detected (Fig. 1). At annealing temperatures higher than 300 °C, the interference fringes apparently disappear and the transmittance minimum becomes deeper. For all the samples in this group, the absorption peak is detected on the range of 610–640 nm, which is characteristic of the SPR of the TiO_2:Au samples.[24,25] The different optical properties of the two groups of films correlate with the XRD patterns of Fig. 5. The growth of gold NPs, occurring already

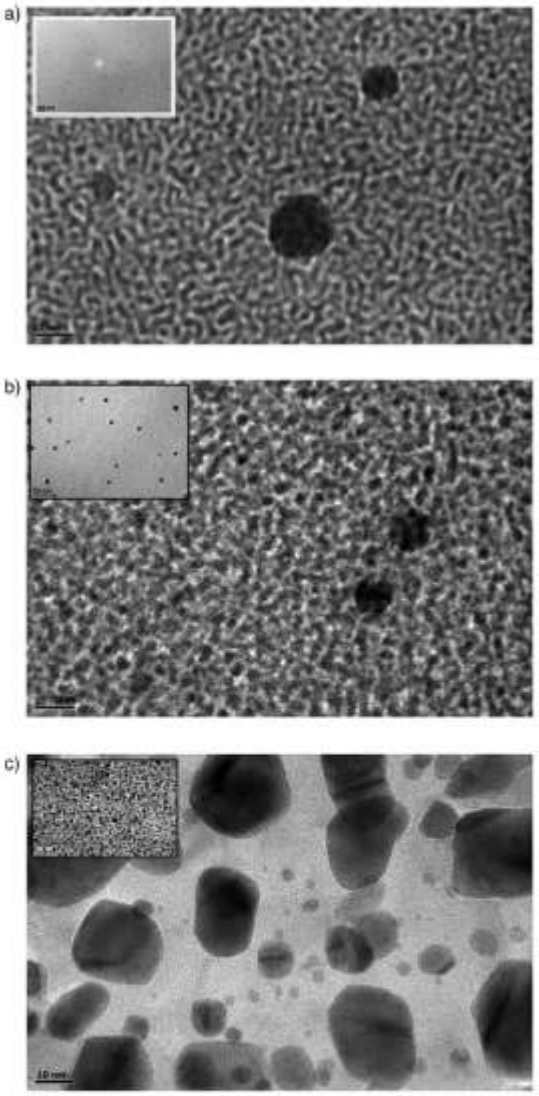

FIG. 2. (a) Planar TEM view of the as-deposited sample. (b) Planar TEM view of the sample annealed at 500 °C showing growing gold NPs. (c) Planar TEM view of the sample annealed at 700 °C showing the formation of larger and elongated NPs.

at 300 °C, is manifested by the observation of the Au face centered cubic (fcc) phase structure [ICDD card n° 04-0787]. The diffraction peaks located at $2\theta = 38.2°$ and $2\theta = 44.4°$ are consistent with the (111) and (200) planes of the Au fcc-type structure. These two peaks become narrower and more intense with the increase of the annealing temperature, which is also consistent with the already mentioned growth of the Au particles observed in Fig. 2. The XRD data of Fig. 5 also show clear evidence of the crystallization of the TiO_2 matrix in the anatase phase [ICDD 21-1272] at 500 °C.[26,27] With further increase of the annealing temperature,

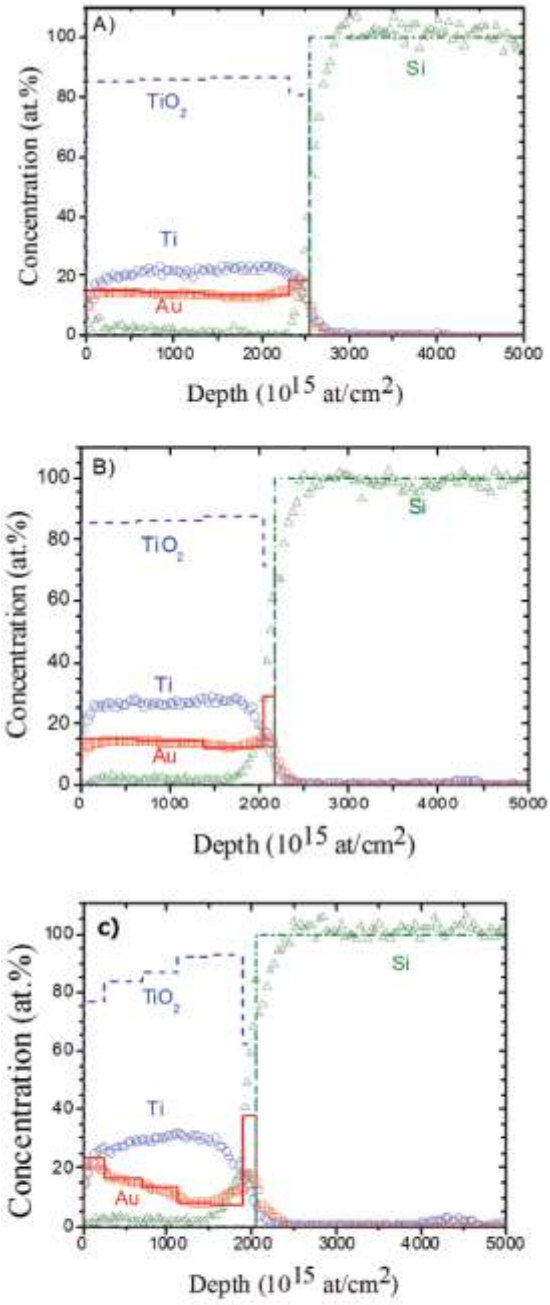

FIG. 3. (Color online) Concentration profiles of different components in different samples, as-deposited (a) annealed at 700 °C (b) and 800 °C (c) obtained by RBS.

the TiO_2 anatase crystallites transform into rutile-type structure [ICDD 21-1276]. Both phases coexist in the second and third groups of samples, and only at 800 °C the transformation seems to be complete. The gradual change of the TiO_2 matrix, from amorphous to crystalline with different phases

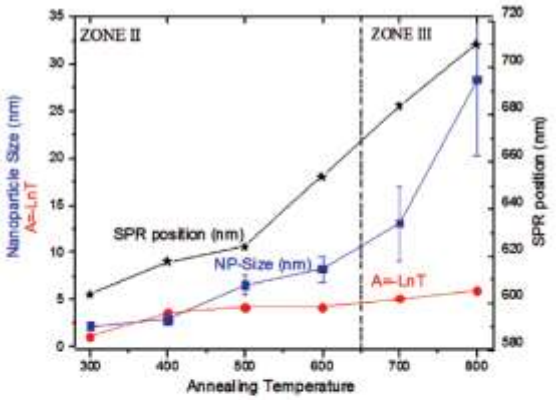

FIG. 4. (Color online) Comparison of the transmission spectra and nanostructure of the samples. The transmittance is presented in logarithmic scale together with the NP size and its standard deviation, and SPR peak position.

dominating as the annealing temperature grows, results in an increase of its dielectric constant[24,28] affecting the SPR effect.

Finally, let us consider the features of the samples annealed at 700 and 800 °C, constituting the third group of samples, denoted as Zone III in Fig. 4. Our TEM analysis revealed quite a different morphology of these two samples, compared to the groups I and II, as can be seen in Fig. 2(c). This figure reveals some tendency of change of the NP's shape, most likely owing to their coalescence. It seems that NPs become elongated (and also bigger). Even though a 3D morphology analysis would be required to confirm it, this conclusion is supported by the optical data, namely, by the shape of the SPR band as discussed in the next section. Also to notice that for these samples, a diffusion-segregation process starts to occur, leading to the accumulation of gold near the surface and at the film-substrate interface, as manifested by the RBS results of Fig. 3.

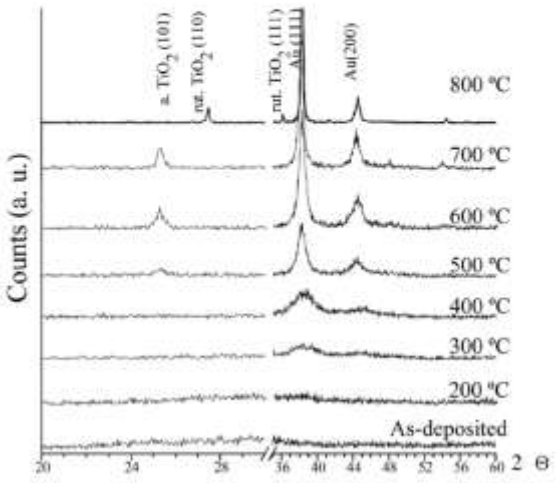

FIG. 5. XRD patterns of the annealed TiO_2/Au films.

The changes in the absorption spectra, which accompany the morphological and structural changes induced by the annealing process, can also be confirmed by the changes in the color coordinate values measured on the CIEL*a*b* scale[29,30] (see Fig. 6). The evolution of the CIEL*a*b* coordinates is also in accordance with the three different zones of annealing temperature, previously identified for the transmission spectra. The changes are particularly clear as far as the a* parameter is concerned. Zone I samples show an undefined interference-type color that changes to red-brownish after annealing treatments at higher temperatures (Zone II). Red ($a^* > 0$) and yellow ($b^* < 0$) colors appear with the increase of the annealing temperature. At the highest annealing temperatures (Zone III), a change in the trend is observed. First, the b* values start to decrease, which is also followed by a drop of the a* value at 800 °C. Simultaneously, the L* value (Lightness) increases significantly and a goldenlike color starts to prevail.

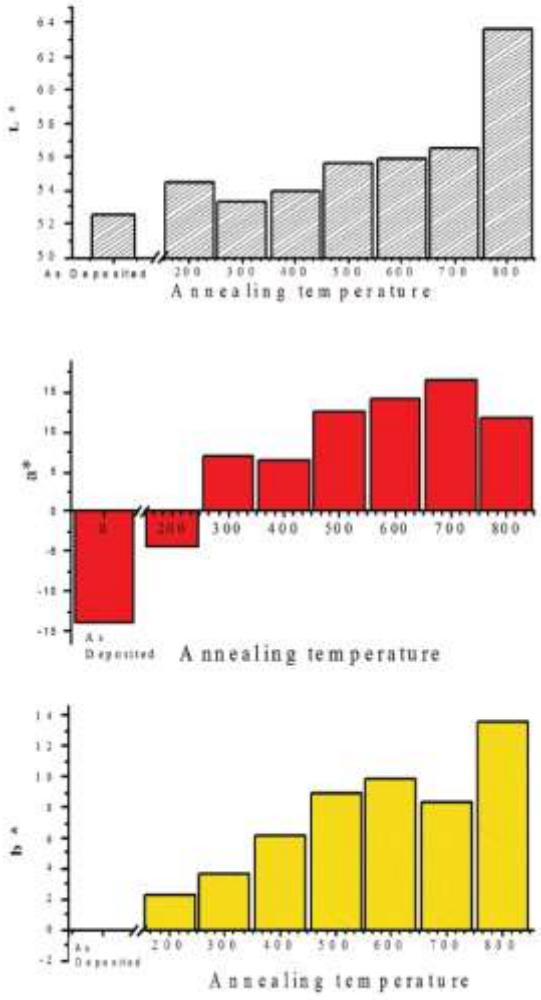

FIG. 6. (Color online) CIELab measurements of the samples annealed at different temperatures.

IV. OPTICAL SPECTRA MODELING

A. Theoretical background

In order to understand the observed correlation between the morphological and structural data and the optical spectra of the nanocomposite films, we performed a theoretical modeling of the latter, based on the concept of effective dielectric function and using the approaches known in the optics of composite and layered media. We begin this part by presenting the essential relations and highlighting the underlying physics.

If the wavelength of the electromagnetic radiation is large compared to both the particle size and the inter-particle distance, the composite medium can be described by an effective dielectric function (EDF). There are two well-known mean-field theories for the EDF calculation, proposed by Maxwell-Garnett and by Bruggemann. The first one is valid in the low-concentration limit (volume fraction of the particles $f << 1$) while the second, on the contrary, can be applied when both f and $(1-f)$ are not too small (see, e.g., Refs. 31 and 32 for discussion). For $f \approx 0.1$, which is our situation, none of these classical approximations is suitable. The Maxwell-Garnett (MG) approximation (assuming independent polarisable particles) can be improved and, consequently, extended to higher f by taking into account the dipole-dipole interactions between the particles.[33,34] This formalism will be hereafter referred to as renormalized MG (RMG) approximation since it considers a renormalized (by the interactions) polarizability of the particles (Eq. 5). It is conceptually equivalent to the average T-matrix approximation known in the theory of disordered media.[32] The RMG approach has been generalized to nonspherical particles in Ref. 33.

An individual particle, polarized by the external electromagnetic field but not interacting with other particles, is described by a bare polarizability tensor with the principal components given by

$$\alpha_i = \frac{\varepsilon_i/\varepsilon_h - 1}{(\varepsilon_i/\varepsilon_h - 1)\,\eta_i + 1}\left(\frac{V}{4\pi}\right),\ i = 1,\ 2,\ 3. \tag{5}$$

Here V is the particle volume and η_i are the depolarization coefficients mentioned in the Introduction (two of them coincide if the particle possesses axial symmetry). For a spheroid with (small) eccentricity e, they are given by[20]

$$\eta_\perp = \frac{1}{3} \mp \frac{1}{15}e^2,\ i = 1,\ 2;\ \eta_\parallel = \frac{1}{3} \pm \frac{2}{15}e^2,\ i = 3, \tag{6}$$

where the two signs correspond to the prolate (elongated) and oblate shape, respectively.

Within the classical MG approximation, the effective dielectric function, ε^*, of the composite medium containing a small fraction of separate inclusions is obtained from the relation,

$$\frac{\varepsilon^* - \varepsilon_h}{\varepsilon^* + 2\varepsilon_h} = \frac{4\pi}{3}N\bar{\alpha}, \tag{7}$$

where $N = f/V$ is the particle's concentration and $\bar{\alpha} = \sum_i \alpha_i/3$. The dipole-dipole interaction between the particles renormalizes their average polarizability, which becomes[33]

$$\alpha^* = \frac{2\bar{\alpha}}{\gamma}\left\{1 - \frac{\sqrt{1-\gamma(1-\delta)}}{2}\left[\sqrt{1-v^2} + \frac{\arcsin(v)}{v}\right]\right\}, \tag{8}$$

where $v^2 = 3\gamma\delta/[1-\gamma(1-\delta)]$, $\gamma = f(4\pi\bar{\alpha}/3V)^2$ and $\delta = \pm(e^2/15)[(\varepsilon_s/\varepsilon_0 - 1)/(\varepsilon_s/\varepsilon_0 + 2)]$. Note that $\alpha^* \to \bar{\alpha}$ when $f \to 0$. Equation (8) is valid for uniform size particles and the more sophisticated formulae taking into account the NP size dispersion can be found in Ref. 33. The effective dielectric function within the RMG approach is calculated by Eq. (7) with α^* replacing $\bar{\alpha}$. Once the dielectric function $\varepsilon^*(\omega)$ is described it is possible to calculate the optical properties of the thin film nanocomposites. For thin films has to be taken into account the eventual multiple reflections at the interface(s), causing the interference effect also detected on this materials for low concentrations of nanoparticles or smallest sizes. When the dielectric functions of the film and the substrate are known, the most convenient method is to use the transfer matrix formalism to calculate the transmission and reflection spectra (see, e.g., Ref. 35).

B. Calculated spectra

The formalism outlined above has been applied to the modeling of the optical spectra of TiO_2/Au composites. First, we present results calculated for a semi-infinite medium, in order to demonstrate the effect of Au nanoparticle size (R), shape (eccentricity, related to the aspect ratio of the spheroid, ξ, according to $e = \sqrt{\xi^2 - 1}$), and the filling fraction (f), not obscured by the influence of the multiple reflections. After this, we turn to the real samples.

For the modeling purposes, a semiempirical relation for the complex dielectric function of gold was used where two extra contributions, $G_1(\omega)$ and $G_2(\omega)$, representing interband transitions were added to the Drude part (Eq. (2)). Both extra terms are of the form,[35]

$$G_l(\omega) = C_l\left[\frac{\exp(i\phi_l)}{(\omega_l - \omega - i\gamma_l)} + \frac{\exp(-i\phi_l)}{(\omega_l + \omega + i\gamma_l)}\right], \; l = 1, 2, \tag{9}$$

with the transition frequencies and the parameters C, φ and γ given in Ref. 36. For the Drude term, we took $\hbar\omega_p = 6.91$ eV and $\varepsilon_\infty = 1.53$. We also considered the size-dependent plasmon damping parameter according to[37]

$$\begin{aligned}\hbar\Gamma_p(R) &= \hbar\Gamma_p(\text{bulk}) + g_s v_F/R \\ &= 0.0244 + 0.922 g_s/R \quad [\text{eV}],\end{aligned} \tag{10}$$

where v_F is the Fermi velocity, g_s is a geometrical factor of the order of unity and R is in nanometers. For the geometrical factor, a value of $g_s \approx 0.7$ has been suggested.[38]

Dispersion of the refractive index of the TiO_2 matrix was taken into account according to the semiempirical relations of Refs. 36 and 39 for rutile and anatase phases, respectively. For amorphous TiO_2 (titania), the refractive index is known to be lower than for the crystalline phases. According to Ref. 40, its value for $\lambda = 550$ nm is between 2.0 and 2.2, compared to 2.903 for rutile and 2.488 for anatase,[41] but no dispersion relation is available for titania. It was generated by assuming a certain volume fraction of the crystalline TiO_2 phases and voids and using the Bruggemann approximation. The calculated value of $n_h(\lambda = 550\text{ nm})$ has been used as a reference fitting parameter.

Calculated absorption spectra are presented in Figs. 7–9. As one can see from Fig. 7, the dipole-dipole interaction (taken into account within the RMG approach) becomes increasingly important as the volume fraction of Au NPs increases. All the other results were obtained using the RMG approximation.

Figure 8 shows that a decrease of the mean NP radius, $\langle R\rangle$, results in a broader absorption spectrum while the peak position remains practically unshifted. Contrary to what one might expect, size dispersion does not produce an additional inhomogeneous broadening of the absorption band (as it is typical of semiconductor nanoparticles). On the contrary, the absorption peak becomes slightly narrower and higher. For the same $\langle R\rangle$, a broader size distribution increases the number of large NPs, that have stronger absorption (notice that $\bar{\alpha}$ is proportional to the volume), and are characterized by a smaller homogeneous broadening (Eq. (10)).

Figure 9 demonstrates the effect of the shape of the NPs on the SPR. It is clearly seen that there are two separate resonances already for moderately elongated NPs ($e = 0.75$ corresponds to an aspect ratio of just 1.25). For nanorods $\eta_{||} \to 0$ and the low-frequency SPR should be strongly redshifted with respect to ω_{SPR} characteristic of spherical NPs.

Now let us consider the real structures, i.e., composite thin films on either glass or quartz substrates. As it has been mentioned above, the calculation of their optical spectra requires the frequency dependent dielectric function for the substrate. We used the expression and parameters proposed in Ref. 42 for the complex dielectric function of silica glass. For quartz, we considered the real part of the complex dielectric function according to the three-term Sellmeier equation[43] and neglected its imaginary part in the

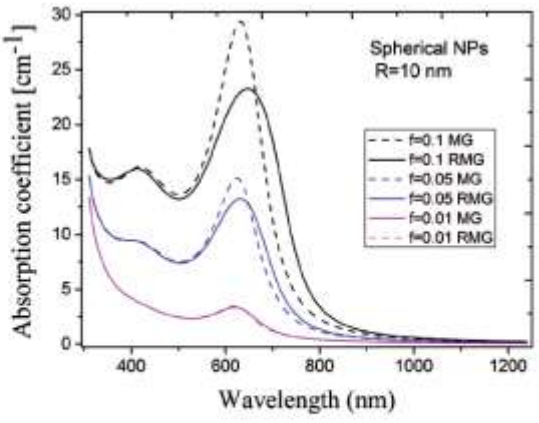

FIG. 7. (Color online) Absorption spectra of composites with different volume fraction of Au spherical NPs of 10 nm in radius, calculated using the standard MG and RMG approximations. $n_h(\lambda = 550\text{ nm}) = 2.4$.

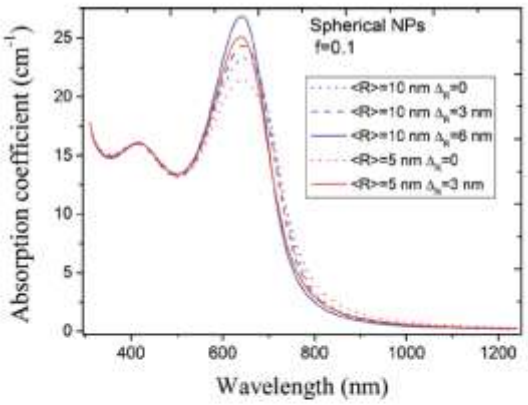

FIG. 8. (Color online) Calculated absorption spectra of composites containing Au spherical NPs of different mean radius $\langle R \rangle$ and its standard deviation as indicated. Au volume fraction $f = 0.1$. $n_s(\lambda = 550\ \text{nm}) = 2.4$.

ultraviolet region which is beyond the spectral range considered here. The fitting results for two samples are presented in Fig. 10 and the corresponding fitting parameters are listed in Table I. For the 800 °C sample we attempted to take into account the segregation of Au near the interface by dividing the film into sub-layers with different values of f, similar to the procedure used in Ref. 44. However, no significant effect on the transmission spectra was obtained. Another effect included in the model for this sample, also related to gold diffusion at high temperature, is the (weak) absorption in the substrate, in the near-infrared (NIR) range. Comparing the NIR part ($\lambda > 900$ nm) of the spectra of two samples in Fig. 10, we notice the higher absorption of the 800 °C one. We associate this absorption with the Au ions penetrating the substrate and modeled it by adding a Lorentzian imaginary part to the dielectric constant of quartz,

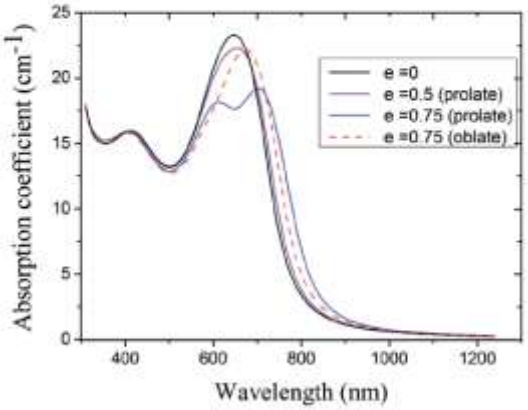

FIG. 9. (Color online) Calculated absorption spectra of composites containing Au NPs of spherical shape with different eccentricity as indicated. Uniform NP radius $R = 10$ nm, Au volume fraction $f = 0.1$. $n_s(\lambda = 550\ \text{nm}) = 2.4$.

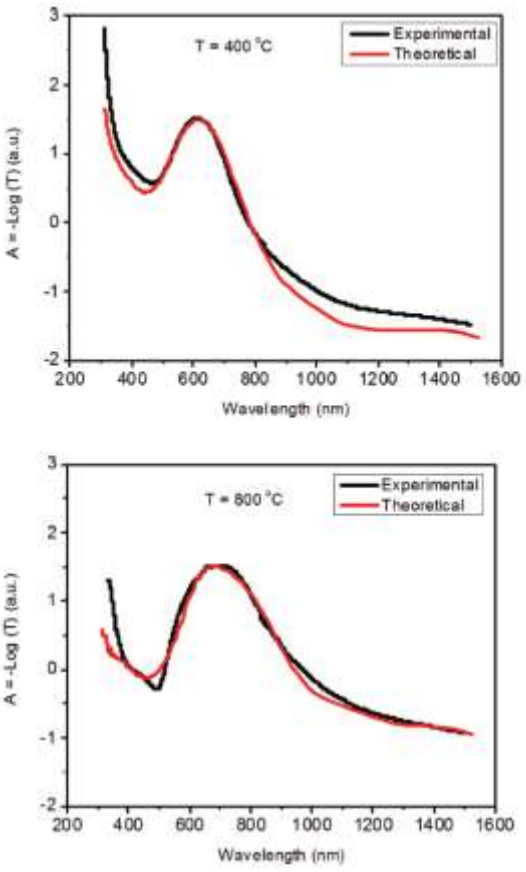

FIG. 10. (Color online) Theoretical and experimental optical transmission spectra (plotted in logarithmic scale) of two TiO_2/Au films annealed at different temperatures.

$$\text{Im}\varepsilon_{\text{sub}}(\omega) = \frac{A\Gamma}{\pi\left[(\omega_0 - \omega)^2 + \Gamma^2\right]} \tag{11}$$

with $\hbar\omega_0 = 0.9$ eV, $\hbar\Gamma = 0.3$ eV and $A = 1 \cdot 10^{-3}$ eV.

Given the complexity of the system, the agreement between theory and experiment in the spectra of Fig. 10 is quite good. From Table I it is obvious that the samples annealed at higher temperature contain larger Au NPs, in agreement with our experimental results presented in Sec. III. According to the fitting, the film annealed at higher temperature experienced a 15% loss of gold, probably due to the segregation and outward diffusion effects. The effective dielectric constant of the matrix is higher for the 800 °C sample due to the change of its phase composition of matrix (rutile rather than anatase). The increased ε_s causes the shift of SPB peak toward the lower energy region. The shape of the gold particles represented by the eccentricity has also been changed for the samples annealed at higher temperature. The NPs are almost spherical when the sample is annealed at 400 °C but they become elongated after annealing at 800 °C.

TABLE I. Parameters used for the calculation of spectra presented in Fig. 10.

Temperature Parameter	400 °C	800 °C
Film thickness (nm)	400	400
Volume fraction of gold (%)	12.5	10.5
Radius of Au particles (nm)	12	15
Eccentricity	0	0.6
$n_h^2(\lambda = 550\ \text{nm})$	5.06	7.12

It results in the splitting of the resonance into two (Fig. 9), appearing as broadening of the absorption band for the higher temperature sample (Fig. 10). Let us stress the importance of taking into account the multiple reflections at the film/substrate interface, since this is the only way to reproduce the transmission spectra outside the strong absorption region.[45]

V. DISCUSSION AND CONCLUSION

Comparing globally the experimental and calculated results for different groups of samples, we can conclude that as grown and low-temperature (zone I) annealed TiO_2/Au composite films do not possess SPR absorption because there are just clusters of a few Au atoms (<1 nm, not detectable by XRD) present in these samples. Higher annealing temperatures (corresponding to zones II and III) are required to produce gold NPs and, consequently, the SPR effect on the optical spectra. Such annealing treatments affect both the TiO_2 matrix, in what concerns its crystalline/amorphous structure and phase composition, and the metallic phase, not only changing the NP size but also the shape. These changes are evidenced by the TEM images presented in Figs. 2(a)–2(c), XRD data of Fig. 5 and the optical parameters summarized in Fig. 4. The experimental data are strongly supported by the modeling results indicating that the redshift of the SPR band is mainly produced by the change of the dielectric constant of the host material due to its crystallization and the rutile phase onset, while the band broadening is caused by the break of the spherical symmetry of the NPs leading to the splitting of the SPR frequency ($\omega_{SPR}^{I} < \omega_{SPR} < \omega_{SPR}^{II}$). The growth of elongated NPs is characteristic of samples annealed at 700–800 °C (zone III in Fig. 4) and probably is related to the coalescence of smaller NPs. We stress that the increase of the size of the NPs leads to the growth of the SPR intensity but does not affect its position, as long as the characteristic wavelengths are much larger than $\langle R \rangle$ and the typical inter-particle distance.

Thus, the results presented show that the characteristics of the SPR resonance can be tuned by choosing the appropriate annealing temperature, namely, it is possible to change the SPR position in the range of approximately 610–710 nm and also the width of the absorption band. This result in changes of the visual appearance of the annealed samples,[44] quantified in terms of their color coordinates (Fig. 6), making the composite TiO_2/Au films attractive for decorative coatings. The SPR absorption appears after annealing treatments at temperatures higher than 300 °C. The SPR band becomes broader for higher temperatures, which can be useful for certain applications, e.g., those involving SERS.[13] However, we would like to point out that the increase of the annealing temperature to or above 800 °C leads to some additional (and probably undesired) effects, such as the segregation of gold at the surface and interface and its penetration into the substrate. These diffusion effects of the Au nanoparticles deserve a separate study.

To conclude, we have shown that the "one step" co-sputtering of a Ti-Au target, followed by an appropriate thermal treatment, is a useful way to produce composite TiO_2/Au films with adjustable nanostructure and, consequently, controllable SPR-related optical properties and color. The factors allowing for such control include the growth of differently shaped gold nanoparticles and the change in the crystallinity and phase composition of the matrix. The NP growth can be monitored by XRD and TEM. The optical properties of the composite films with NP volume fraction of the order of 0.1 are well described by the renormalized Maxwell-Garnett approximation for the effective dielectric function,[32,33] combined with the standard multilayer optics approach.

ACKNOWLEDGMENTS

The authors acknowledge the Portuguese Foundation for Science and Technology (FCT) for the financial support through project PTDC/CTM/70037/2006 funded under the program "Programa Operacional Factores de Competitividade (COMPETE)" from "Quadro de Referência Estratégico Nacional (QREN)" co-participated by FEDER.

[1] H. Takele, H. Greve, C. Pochstein, V. Zaporojtchenko, and F. Faupel, Nanotechnology **17**, 3499 (2006).
[2] E. Hutter and J. H. Fendler, Adv. Mater. **16**, 1685 (2004).
[3] G. Walters and I. P. Parkin, J. Mater. Chem. **19**, 574 (2009).
[4] M. Torrell, P. Machado, L. Cunha, N. M. Figueiredo, J. C. Oliveira, C. Louro, and F. Vaz, Surf. Coat. Technol. **204**, 1569 (2010).
[5] J. Lian, L. M. Wang, R. C. Ewing, and L. A. Boatner, Nucl. Inst. Methods Phys. **B242**, 448 (2006).
[6] C. Pacholski, A. Kornowski, and H. Weller, Angew. Chem. Int. Ed. **43(36)**, 4774 (2004).
[7] J.-J. Wu and C.-H. Tseng, Appl. Catal. B **66**, 51 (2006).
[8] Y. Li, Y. Hu, S. Peng, G. Lu, and S. Li, J. Phys. Chem. C **113**, 9352 (2009).
[9] M. Z. Atashbar, H. T. Sun, B. Gong, W. Wlodarski, and R. Lamb, Thin Solid Films **326**, 238 (1998).
[10] R. M. Walton, D. J. Dwyer, J. W. Schwank, and J. L. Gland, Appl. Surf. Sci. **125**, 187 (1998).
[11] M.G. Manera, J. Spadaveecchia, D. Buso, C. de Julián Fernández, G. Mattei, A. Martucci, P. Mulvaney, J. Pérez-Juste, R. Rella, L. Vasanelli, and P. Mazzoldi, Sens. Actuators B **132**, 1, 28107 (2008).
[12] F. Hache, D. Richard, C. Flytzanis, and K. Kreibig, Appl. Phys. A. **47**, 347 (1988).
[13] K. Kim, H. B. Lee, J.K. Yoon, D. Shin, and K. S. Shin, J. Phys. Chem. C **114**, 13589 (2010).
[14] D. Dalacu and L. Martinu, J. Vac. Sci. Technol. A **17**, 877 (1999).
[15] S. H. Cho, S. Lee, S. Ghee, S. Jin Park, W. Mok Kim, B. Cheong, M. Chung, K. B. Song, T. S. Lee, and S. G. Kim, Thin Solid Films **377**, 97 (2000).
[16] D. Dalacu and L. Martinu, J. Appl. Phys. **87**, 228 (2000).
[17] C. F. Bohren and D. R. Huffman, *Absorption and Scattering of Light by Small Particles* (Wiley, New York, 1998).
[18] G. Mie, Ann. Phys. **25**, 377 (1908).
[19] J. Rodriguez-Fernandez, C. Novo, V. Myroshnychenko, A. M. Funston, A. Sánchez-Iglesias, I. Pastoriza-Santos, J. Pérez-Juste, F. J. García de Abajo, L. M. Liz-Marzán, and P. Mulvaney, J. Phys. Chem. C **113**, 18623 (2009).

[21]L. D. Landau and E. M. Lifshitz, *Electrodynamics of Continuous Media* (Pergamon, Oxford, 1984).
[22]T. Ung, L. M. Liz-Marzan, and P. Mulvaney, J. Phys. Chem. B **105**, 3441 (2001).
[23]N. P. Barradas, C. Jeynes, and R. P. Webb, Appl. Phys. Lett. **71**, 291 (1997).
[24]A. R. Ramos, A. Paúl, L. Rijniers, M. F. da Silva, and J. C. Soares, Nucl. Instr. Meth. B **190**, 95 (2002).
[25]M. Lee, L. Chae, and K. C. Lee, Nanostruct. Mater. **11**, 195 (1999).
[26]M. Torrell, L. Cunha, A. Cavaleiro, E. Alves, N. P. Barradas, and F. Vaz, Appl. Surf. Sci. **256**, 6536 (2010).
[27]M. Hasan, A. Haseeb, R. Saidur, H. Masjuki, and M. Hamdi, Opt. Mater. **32**, 690 (2010).
[28]N. Martin, C. Rousselot, D. Rondot, F. Palmino, and R. Mercier, Thin Solid Films **300**, 113 (1997).
[29]D. Buso, J. Pacifico, A. Martucci, and P. Mulvaney, Adv. Funct. Mater. **17**, 347 (2007).
[30]*Colorimetry*, CIE Publ. 15 (Commission Internationale de L'Éclairage, Paris, 1971).
[31]*Recommendations on Uniform Color Spaces, Difference–difference equations, psychometric color terms*, CIE Publ, (Commission Internationale de L'Éclairage, Vienna, 1986).
[32]L. Genzel, and U. Kreibig, Z. Phys. B **37**, 93 (1980).
[33]V. M. Shalaev, *Nonlinear Optics of Random Media* (Springer, Berlin, 2000).
[34]M. I. Vasilevskiy and E. V. Anda, Phys. Rev. B. **54**, 5844 (1996).
[35]M. I. Vasilevskiy, Phys. Stat. Sol. B **219**, 197 (2000).
[36]E. Malainho, M. I. Vasilevskiy, P. Alpuim, and S. A. Filonovich, J. Appl. Phys. **106**, 073110 (2009).
[37]P. G. Etchegoin, E. C. Le Ru, and M. Meyer, J. Chem. Phys. **125**, 164705 (2006).
[38]E. D. Palik, *Handbook of Optical Constants of Solids* (Academic Press, New York, 1985), Vol. 1.
[39]H. Baida, P. Billaud, S. Marhaba, D. Christofilos, E. Cottancin, A. Crut, J. Lermé, P. Maioli, M. Pellarin, M. Broyer, N. Del Fatti, and F. Vallée, Nano Lett. **9**, 3463 (2009).
[40]A. R. Forouhi and I. Bloomer, Phys. Rev. B **34**, 7018 (1986).
[41]D. Mergel, D. Buscendorf, S. Eggert, R. Grammes, and B. Samset, Thin Solid Films **371**, 218 (2000).
[42]G. B. Song, J. K. Liang, F. S. Liu, T. J. Peng, and G. H. Rao, Thin Solid Films **491**, 110 (2005).
[43]D. Franta, D. Necas, and L. Zajickova, Opt. Exp. **15**, 16230 (2007).
[44]I. H. Malitson, J. Opt. Soc. Am. **55**, 1205 (1965).
[45]T. Polcar, T. Kubart, E. Malainho, M. Vasilevskiy, N. Parreira, and A. Cavaleiro, Nanotechnology **19**, 395202 (2008).
[46]M. Torrell, L. Cunha, M. R. Kahir, A. Cavaleiro, M. I. Vasilevskiy, and F. Vaz, Mat. Lett. **64**, 2624 (2010).